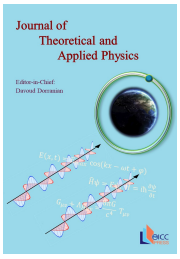

Volume 17, Issue 2, 172322 (1-9)

Journal of Theoretical and Applied Physics (JTAP)

https://dx.doi.org/10.57647/j.jtap.2023.1702.22

Dopant and milling time effect on impedance and electrical properties of perovskite ceramics

Shristi Chaudhary[1], Mikanshi Chaudhary [1], Sheela Devi [2]*, Shilpi Jindal [1]

[1]*Department of Physics, Chandigarh University, Gharuan, Mohali, Punjab, India.*
[2]*Department of Applied Sciences, MSIT, C-4, Janakpuri, New Delhi, India.*

***Corresponding author**: physics.sheela@gmail.com

Received 30 November 2022; Accepted 23 February 2023; Published online 27 February 2023

Abstract:
Tungsten doped Barium Titanate (BT) with composition $BaW_{0.05}Ti_{0.95}O_3$ (BWT) were prepared by using ball milling technique for different hours (10 h, 20 h and 30 h). In the present paper, the microstructural, dielectric and impedance studies are discussed. The microstructural studies using XRD data reveals the formation of single phased tetragonal structure and perovskite structure. The dielectric properties of BT nanoceramics were significantly enhanced by the partial replacement of W (at B site) showing the diffuse phase transition at 80°C. Dielectric loss rises as the temperature rises. There is increase in charge carrier mobility which results in increased polarization and significant dielectric loss. Additionally, compared to the un-milled BWT ceramic sample, the 30 h milled had superior dielectric characteristics with high dielectric constant and reduced loss. The nature of the phase transition was confirmed by the Curie-Weiss law and the ferroelectric analysis was carried by well-established P-E loops. The impedance studies were carried out by plotting Nyquist plots. The ac conductivity plot follows Arrhenius relation and the calculated activation energy confirms the negative temperature coefficient of resistance (NTCR) behavior of the material.

Keywords: Ferroelectrics, Barium titanate, XRD, SEM, PE, Dielectric, Impedance spectroscopy

1. Introduction

Barium titanate (BT) is one of the well-known and widely studied lead free ferroelectric and piezoelectric material having curie temperature around 120°C with tetragonal structure. Above this temperature BT behaves as a para-electric material and shows cubic structure. Many studies have already stated that BT has fascinating dielectric and ferroelectric properties with different known applications such as multilayer capacitors, storage devices, actuators, transducers, thermistors, and sensors, so it is not a novel material [1-5]. $BaTiO_3$ is a lead-free environment friendly perovskite material (ABO_3 type structure as shown in Figure 1 using VESTA software, where Ba occupies the A site and Ti occupies for B site), making it a good alternative for lead-containing materials in a variety of applications including electro-optical and electronics [6, 7].
There are several ways to synthesize nanosized BT, including the hydrothermal approach, the sol–gel procedure [8, 9], the solid-state reaction [10], hydrothermal method [11]and the chemical coprecipitation [12]. Pure Barium titanate behaves as electric insulator at room temperature but different dopants could be used to change the electrical characteristics of BT such as transition metal doped BT [13, 14], rare earth doped BT [15, 16], alkali doped BT [17, 18].
Several studies have been published on the effects of doping and substituting single transition metal oxides, such as Co [19], Fe [20, 21], Ni [22, 23], and W [24], in the compound $BaTiO_3$. Due to their similar ionic radii W^{6+}(0.60) and Ti^{4+}(0.60), W is generally preferred among all the transition metals that were evaluated to replace $BaTiO_3$ because it anticipated to induce less strain in the compound. A minor deformation of the octahedron occurs because the bond dissociation energy of the W-O bond (653 kJ/mol) is lower than that of the Ti-O bond.[25] Additionally, the W^{6+} ion's higher valence tends to create certain cation vacancies that result in dipolar defects. It is anticipated that the random field surrounding these defects will reduce the activation barrier necessary for the formation of new domains, hence reducing the coercive field's value and assisting domain motion's growth in ferroelectric characteristics. Ahn et al. discussed that the effect of strontium and tungsten on

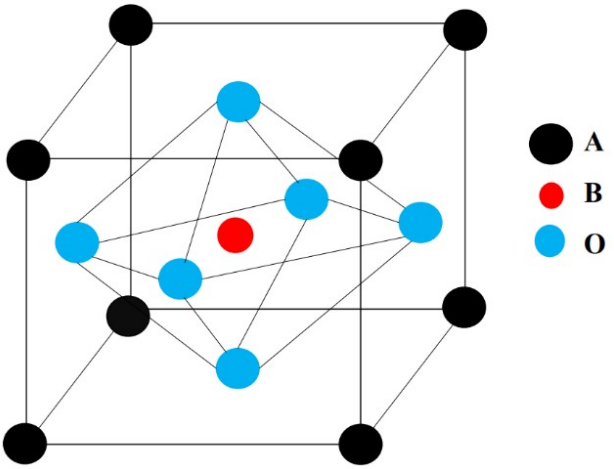

Figure 1. Perovskite structure (ABO_3).

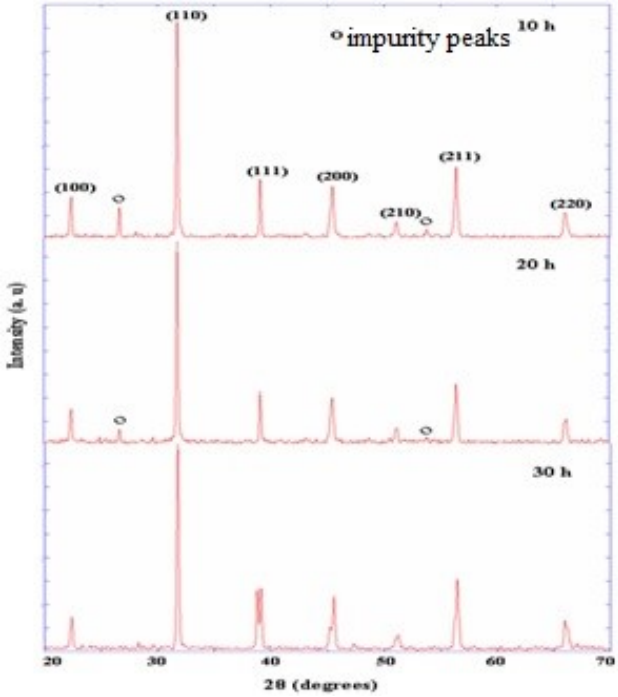

Figure 2. XRD pattern of BWT.

BT prevented a clear transition between the ferroelectric tetragonal and paraelectric cubic structures, making it applicable for ferroelectric devices. [24] According to Devi et al. the charge neutrality of the system allowed substitutional tungsten atoms in the hexavalent state (W^{6+}) in BT to successfully create trivalent titanium (Ti^{3+}) atoms, which effectively improved the ferroelectric characteristics. [26] The effects of tungsten concentration variation on tungsten-doped barium strontium titanate have been investigated by Kavitha et al. According to the study, tungsten doping improves conductivity while simultaneously expanding the band gap and changing the material's morphology from spherical to rod-like. This makes it suitable for its use in dye-sensitized solar cells. [27]

Many studies have found that adding tungsten to Barium titanate improves its electrical properties, as WO_3 has an excellent dielectric constant at room temperature and it is a good ferroelectric material. The enhancement of dielectric and ferroelectric properties has also also reported by many researchers. However, the simultaneous effect of dopant and milling time on the study of impedance and electrical properties of perovskite ceramics has not been understood much and it needs further investigation. Hence, the main focus of the present article is to study the substitution of W^{6+} at B site of Barium titanate to observe its effect on the electrical characteristics of BT ferroelectric ceramics, including complex impedance spectroscopy. The samples were synthesized using ball milling, i.e. without going through a time-consuming calcination process. This technique also gives homogenous grinding of the materials. Compared to the solid-state reaction technique and other preparation procedures, the ferroelectric characteristics of the samples are found to improve. For example, the efficiency increases from 51% to 57% with milling time, the curie temperature reduces (80°C), and the dielectric constant increases from 2358.44 to 2959.89 and then to 3612.18 with increased milling time from 10 hours to 20 hours and then to 30 hours. Also, the samples move from bulk towards nano-range as the milling duration increases, indicating a broad application of the samples in charge storage and tunable devices, confirmed by the estimate of charge storage density from the P-E loops.

2. Materials and method

The sample with the composition $BaW_xTi_{1-x}O_3$, where $x = 0.05$, was synthesized using the ball milling technique. The oxides and carbonates were taken as a starting material from Aldrich, namely $BaCO_3$, TiO_2 and WO_3 with 99.9% purity according to the stoichiometric ratio. These starting materials were weighed and mixed. These powders were mixed for different times (10 hours, 20 hours and 30 hours) in a ball miller to get a homogeneously fine powder. Milled

Table 1. Lattice parameter, Volume, Crystallite size and relative density of BWT.

Milling time	$a(Å)$	$c(Å)$	Volume $(a^2c)(Å)^3$	Crystallite size (D in nm)	c/a	$\rho_r(\rho_m/\rho_t)$ (%)
10 h	3.9945	4.0246	64.216	33.63	1.0075	97.03977
20 h	3.9918	4.0213	64.077	33.78	1.0073	96.82917
30 h	3.9915	4.0197	64.042	33.99	1.0070	96.77609

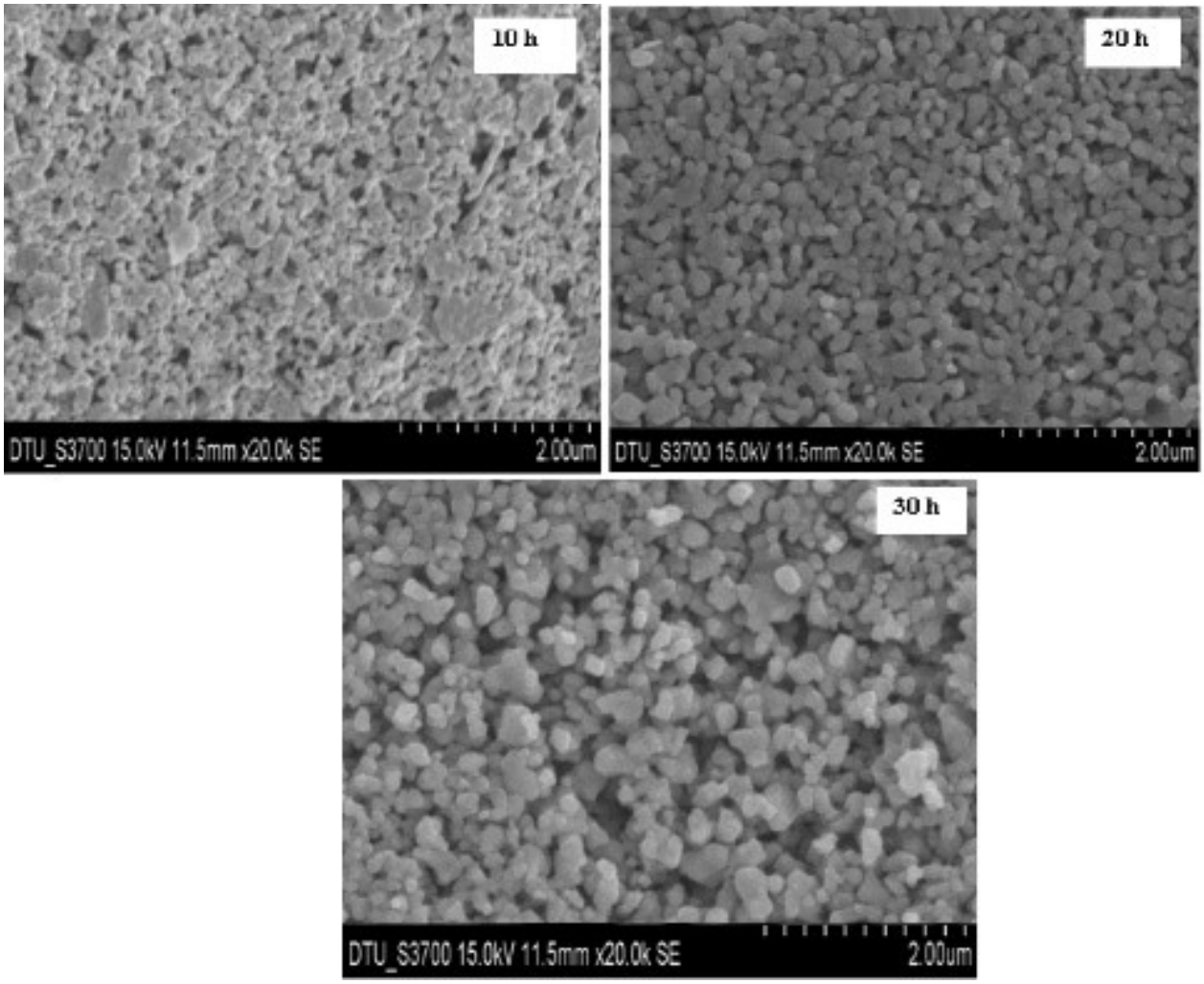

Figure 3. SEM images of BWT.

powders were then heated at 1100°C for 4 hours in a programmable furnace.

On a Philips X-ray diffractometer, an X-ray diffractogram of the sintered sample was recorded using CuKα radiation ($\lambda = 1.540$ Å) at a scanning rate of 0.02 °/s in the range 20° to 70°. The Cambridge Stereo Scan 360 microscope was used to capture a scanning electron micrograph (SEM) of the sample. For dielectric studies, to be used as electrodes, after sintering the pellets were polished to a 1 mm thickness and then both the sides were coated using silver paste and cured at 300°C for 15 minutes. On an Agilent 4284A LCR metre, the dielectric parameter was measured at a 1-Volt oscillation amplitude from 100 Hz to 1 MHz. Using a Keithley 6517A high precision electrometer, electrical measurements were taken from 25°C to 250°C at a heating

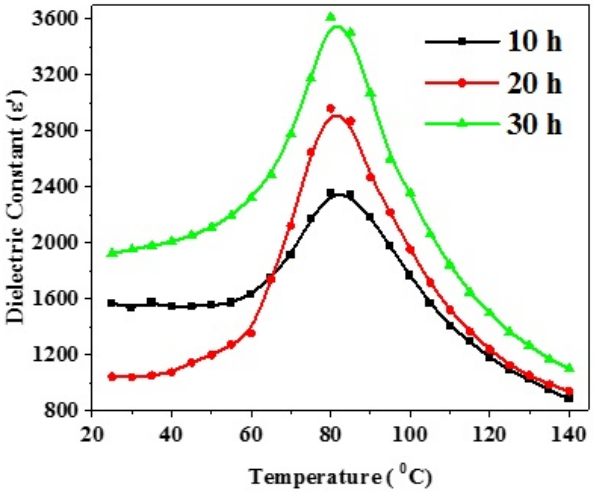

Figure 4. Dielectric Constant versus Temperature of BWT.

Table 2. Values of Curie temperature and Dielectric constant of BWT.

Milling Time	Curie temperature (T_c)	Dielectric constant ($\acute{\varepsilon}$)
10 h	80°C	2358.44
20 h	80°C	2959.89
30 h	80°C	3612.18

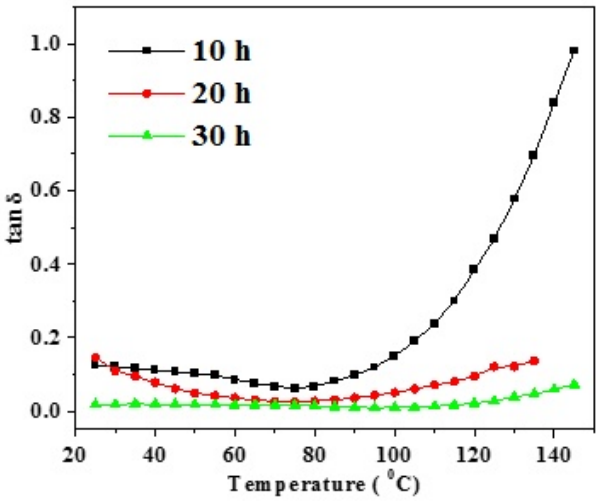

Figure 5. Dielectric loss versus temperature of BWT.

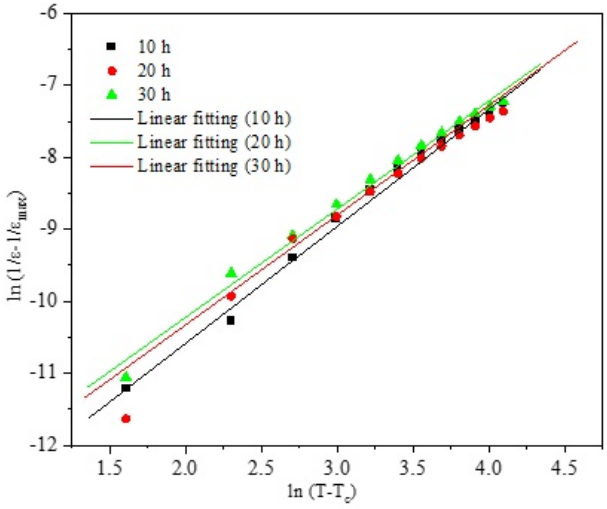

Figure 6. $\ln(1/\varepsilon - 1/\varepsilon_{max})$ versus $\ln(T - T_c)$ of BWT.

rate of 1°C per minute. The impedance measurements were performed using an Agilent 4284A precision LCR meter in the frequency range 100 Hz - 1 MHz in the temperature range 300–500°C at a 50°C interval.

3. Results and discussion

The X-ray diffraction pattern of the investigated material is shown in Figure 2. The XRD studies reveal the formation of single-phase perovskite structure. The most intense peak is found at the angle of 32.17 degrees and the other diffraction peaks are found at 22.208, 32.17, 39.2, 41.2, 45.59, 50.81, 56.7 and 65.77 degrees, which are indexed to the (100), (110), (111), (200), (210), (211) and (220), respectively. In the 10- and 20-hour milling cases, the peaks of TiO_2 phase can be detected at 27.42 and 54.41 degrees but in the 30-hour milling XRD plot, this peak has completely disappeared, suggesting more homogeneity. Additionally, when W is added to pure BT, there is a slight shift of the peaks towards the higher angle in the sample compared to others work, and the intensity of peaks is found to increase. This could be due to the fact that W ions are replacing Ti in the lattice as ionic radii of W is comparable to Ti and Ba. [26, 27] Different parameters, such as lattice parameters and volume, have been calculated from XRD patterns and are mentioned in Table 1. A reduction in the values of lattice parameter is found compared to the reviewed data of Barium titanate due to substitution of tungsten in BT as the tungsten occupying the B-site. [28] The very slight decrease in the values of the volume is observed with increasing milling time. Also, the crystallite size was calculated by the Debye-Scherrer's formula and the variation tells the increase in charge formation and conductivity compared to pure BT. [27] The tolerance factor (t), used by Goldschmidt to account for the cation size limitations necessary to form a perovskite structure [29], is defined as

$$t = \frac{r_A + r_o}{\sqrt{2}(r_B + r_o)} \tag{1}$$

where R_{Ba}, $R_{Ti/W}$, and R_O are, respectively, the ionic radii of the 12-fold coordinated Ba^{2+} ion, the 6-fold coordinated Ti^{4+}/W^{6+} ion, and the 6-fold coordinated O^{2-} ion. Ba^{2+} ($R_{Ba} = 1.61$ Å) and Ti^{4+}/W^{6+} ($R_{Ti} = 0.605$ and $R_W = 0.6$ Å) ionic radii are taken into account, and a tolerance factor of 1.06 is determined for all samples. According to published research, the perovskite structure is stable in the tolerance factor range of 0.880 to 1.090. [29] A value of t close to 1 indicates that the compound is more stable and that the symmetry of the perovskite structure is higher. Tetragonal distortion is favored if the t value is greater than 1, but rhombohedral distortion is preferred if the t value is less than 1. The splitting of the peak at $2\theta = 45.59°$ into (200) and (002) for the tetragonal phase suggests an octahedral distortion in this case. Hence, the tetragonal structure

Table 3. P_r (Remanent Polarization), E_c (Coercive Field), Saturation Polarization (P_s), Discharge density (W_1), Charge storage energy (W_2) and γ (diffusivity) of BWT.

Milling time	Diffusivity (γ)	Remanent Polarization (P_r in μC/cm^2)	Coercive Field (E_c in kV/cm^{-1})	Saturation Polarization (P_s in μC/cm^2)	Discharge density (W_1 in J.cm^{-3})	Charge storage energy (W_2 in J.cm^{-3})	Efficiency Efficiency (η in %)
10 h	1.64	6.573	3.621	13.621	137.68	266.09	51.74
20 h	1.62	6.913	2.644	14.258	175.83	341.33	51.51
30 h	1.50	7.169	2.788	16.476	258.54	457.70	56.48

Table 4. Fitted circuit values from Nyquist plot of BWT.

Milling time	10 h			20 h			30 h		
Equivalent circuit	$(R1+C2/R2)$			$(R1+C2/R2)$			$(R1+C2/R2)$		
Temperature	|300°C	325°C	350°C |	|430°C	455°C	490°C |	|450°C	475°C	500°C|
$R1$ (Ohm)	|3.42	136.9	90.49 |	|8.359	6.992	205.5 |	|111.52	8.932	6.769 |
$C1$ (e^{-3} F)	|5.506	5.177	0.151 |	|1.553	1.579	1.543 |	|2.484	1.543	2.364 |
$R2$ (Ohm)	|132.8	1.836	1.074 |	|407.5	308.3	18.2 |	|239.3	107.2	135.3 |
χ^2	0.9	0.6	0.7	0.9	0.5	0.7	0.7	0.9	0.8

is confirmed from the above information for the studied material.

The well-developed grains can be seen in the SEM images in Figure 3. The size of nanoparticles was in the range of 30-60 nm which is in good agreement with the observed XRD pattern and also porous representation of the grains shows that the doping of W reduces the density of the barium titanate structure, allowing it to be used in sensing devices. The information on the formation of nano grains is provided by the reduction in grain size with milling time. The extremely compact and closely packed particles on the surface morphologies are favorable for the effective generation of charge carriers. The relative density has been calculated by taking ratio of measured ($\rho_m = m/v$) and theoretical density ($\rho_t = ZM/VN$) and listed in the Table 1. [28, 30-31]

Figure 4 illustrates the dielectric constant of the examined material as a function of temperature at a constant frequency (1 MHz). At all frequencies, the phase transition from ferroelectric to paraelectric is observed at the similar value of temperature, commonly known as Curie temperature (T_c), the point where the value of dielectric constant is extreme (maximum), demonstrating non-relaxor behavior and the values of dielectric constant and curie temperature for three different milling hours are shown in Table 2. In comparison to literature of pure BT samples, when titanium is partially replaced by tungsten, the value of curie temperature (T_c) drops to 80°C from 120°C. One of the reasons for the lower dielectric constant value could be the reduction in bonding energy amongst the B-site and the oxygen octahedral of the perovskite structure [26, 32]. The octahedron's distortion is weaker as bonding energy decreases caused by the replacement of tungsten for titanium at the B-site. Furthermore, there is also a drop in the c/a ratio since W has similar ionic radius as compared to Ti. It is also observed that with the doping of W, the value of dielectric constant also increases due to space charge polarization. Additionally, as the material goes through a high-temperature sintering process, there is formation of oxygen ions or oxygen vacancies which is increasing the value of dielectric constant [30, 33]. The tunable devices reported in the present work are applicable to this decrement in curie temperature as well as high dielectric constant. So, moving towards the nanoscale we can say that these ferroelectric material with a wide range of uses in phase shifters, tunable oscillators, and detectors can be used to create electrically tunable devices. [27, 34-36] The dielectric loss plots as a function of temperature at various frequencies are shown in the Figure 5. The graphs display very minor changes and the dielectric loss is mainly unaffected by temperature up to 80°C; after that, it increases as temperature rises. The dielectric loss can be defined as the ratio of imaginary part of permittivity to the real part of permittivity. In theory, three separate phenomena cause dielectric loss in dielectric materials: space charge migration (interfacial polarization contribution), direct current (DC) conduction, and molecule dipole movement (dipole loss). The dielectric constant has been shown to play vital roles in several nonlinear phenomena [37] It is observed from the graph that with increase in tungsten substitution and milling time, the value of dielectric loss decreases. The increase in dielectric loss with respect to temperature for 10, 20 and 30 milling hours may be due to the space charge polarization [30]. The dielectric graphs exhibit that the BWT is showing diffuse nature and the diffusivity of the studied material can

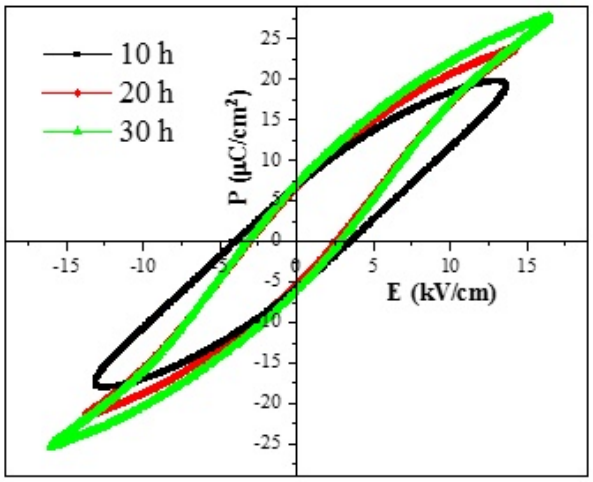

Figure 7. *P-E* loop of BWT.

Table 5. Values of activation energy of BWT.

Milling Time	Activation Energy (E_a)
10 h	0.318
20 h	0.112
30 h	0.428

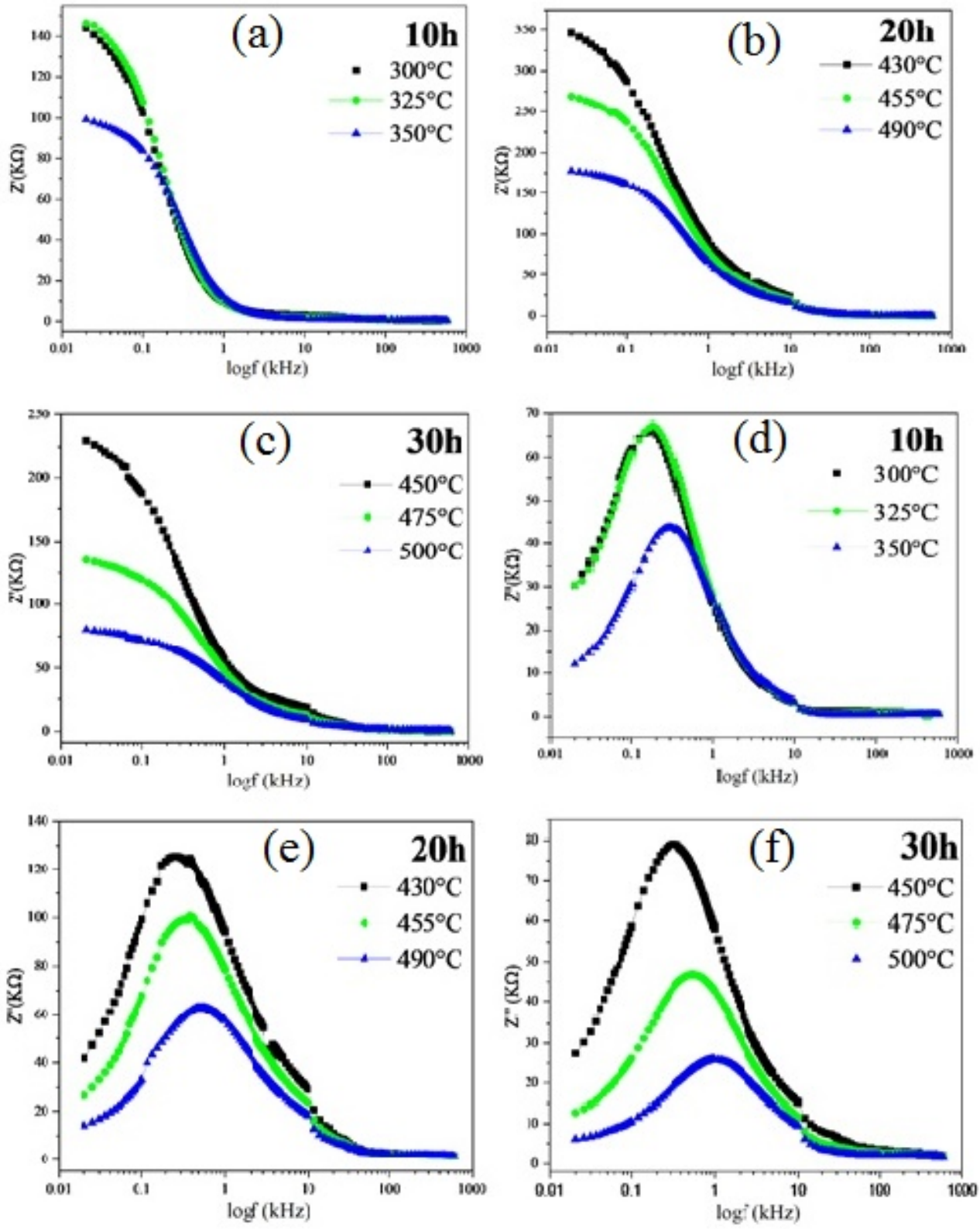

Figure 8. Real part and imaginary part of impedance with Frequency of BWT.

be described by the given formula:

$$\ln[\frac{1}{\varepsilon}-\frac{1}{\varepsilon_{max}}]=\gamma\ln[(T-T_c)+Constant] \qquad (2)$$

The above equation is modified form of Curie–Weiss law for diffusiveness of phase transition where the parameter γ is the diffusivity of the phase transition, and its value is between 1 and 2. So, for $\gamma=1$, a typical Curie–Weiss law is found and it reduces to the quadratic dependency which represents a complete diffuse phase transition (DPT) for $\gamma=2$.

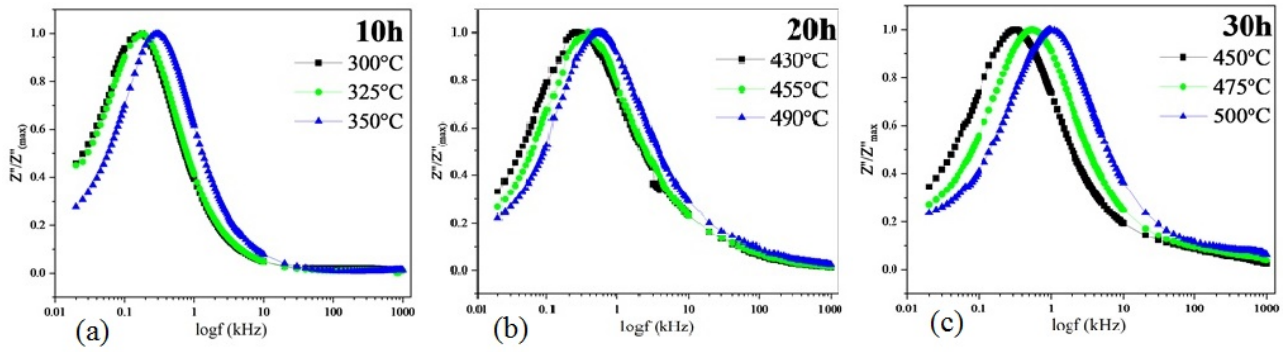

Figure 9. $\acute{Z}/\acute{Z}_{max}$ versus $\log f$ of BWT.

In Figure 6, the plot of $\ln(1/\varepsilon - 1/\varepsilon_{max})$ vs. $\ln(T - T_c)$ at various frequencies reveals a linear nature relationship. The value of diffusivity is computed as shown in the Table 3, and the trend of the values of diffusivity reduces as milling time increases due to a reduction in disorder or impurities. [28]

A *P-E* hysteresis loop as illustrated in Figure 7 was used to investigate the ferroelectric behavior of BWT for different milling time (10 h, 20 h and 30 h) applying a maximum field at room temperature. For each milling time, a well-saturated hysteresis loop was seen, with a slight increase in remnant polarization and the slight decrease in coercive field and the respective values are tabulated in the Table 3. Donor doping of tungsten causes a 'soft' appeal in the material resulting in rise in saturation polarization as the domains move more easily. The BWT's discharge energy density ($W_1 = \int_{p_r}^{p_m} Edp$), charge energy density ($W_2 = \int_{p_0}^{p_m} Edp$), and energy efficiency ($\eta = W_1/W_2$) was computed from *P-E* hysteresis loops for 3 different milling hours and the values are tabulated in Table 3. The pattern of these results indicates that energy storage density and efficiency increase as milling time increases, supporting the increased capacity of using this sample as storage devices. [28, 38]

The complex impedance analysis is a significant and efficient tool in material sciences. It is an effective approach which can determine the contributions of numerous mechanisms including electrode effects, bulk effects, and interfaces, such as grain boundaries, etc. when the relaxation time of distinct mechanisms vary as a result of various capacitance components then the representation of complex impedance is utilised. Complex impedance (Z^*), complex admittance (Y^*), complex permittivity (ε^*), and complex modulus (M^*) are the four formalisms linked to impedance study. The plot in the impedance studies is between the real and imaginary parts of the impedance representing a semi-circular arc. They produce three semi-circular arcs in the complex impedance plot depending on the respective values of their relaxation times. In general, bulk electrical conduction is represented by the high frequency arc, grain boundary conduction by the intermediate (middle arc) arc, and electrode processes by the low frequency arc. The single RC combination can depict these semi-circular arcs. A semicircle with a centre that is lower than the real axis indicates that it is not obeying ideal Debye behaviour. The semicircle satisfies the criterion (i.e., $\omega\tau = 1$) by passing through a maximum at relaxation frequency. The Debye model is a classic model for describing impedance behaviour stated in the formula

$$Z^* = \acute{Z} - j\acute{\acute{Z}} \tag{3}$$

$$Z^* = \frac{R}{1 + i\omega\tau} \tag{4}$$

The value of $\tau = RC$. This equation suggests a simple parallel *RC* circuit that produces a semicircle in the complex plane with its centre on the real axis (Z vs Z) or a Debye peak of the imaginary component of the spectroscopic plots (Z versus $\log f$).

$$\acute{Z} = \frac{R}{1 + (\omega RC)^2} \tag{5}$$

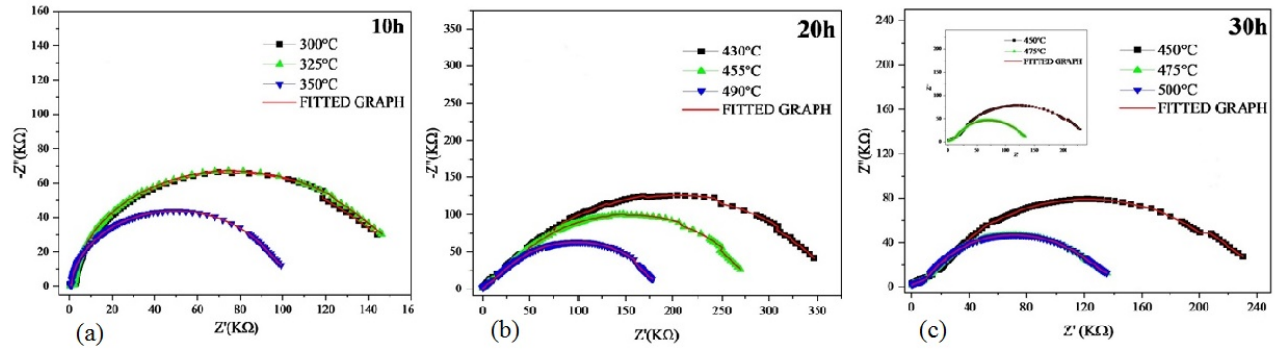

Figure 10. Cole-Cole plots for different milling hours of BWT.

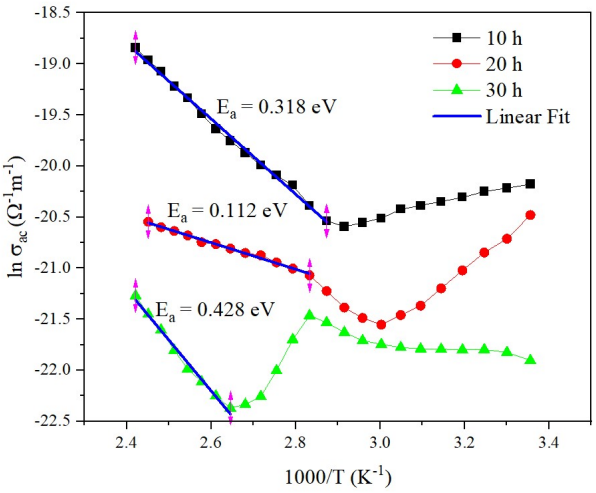

Figure 11. Ac conductivity with inverse of temperature of BWT.

$$\acute{Z} = R\frac{\omega RC}{1+(\omega RC)^2} \tag{6}$$

In order to study impedance spectroscopy, plots of real and imaginary parts of impedance against frequency have been observed at various temperatures for different milling time (10 h, 20 h and 30 h). Figures 8(a), 8(b) and 8(c) depict how the real part of impedance varies with frequency at temperatures ranging from 300°C to 500°C. These figures demonstrate the reduction in impedance with increasing value of frequency. The impedance value is lower for higher temperatures in lower frequency ranges and steadily decreases as frequency is increased, indicating an enhancement in the conduction. The values of real part of impedance of all temperature range merges at higher frequency region which is due to the release of space charge which further supports the enhancement of conduction. The variation of imaginary part of impedance with frequency at various temperature range is shown in Figures 8(d), 8(e) and 8(f) for 10, 20 and 30 milling hours, respectively. The figure displays the peak maximum for different temperatures and there is a slight shifting in the peaks with increase in temperature which is due to mobile charge carriers. Conduction electrons are formed when oxygen vacancies are ionized and can be easily thermally activated and hence, due to conduction, the graphs for different milling times merge in higher frequency region. The broadening of peaks with increasing temperature must be due to relaxation phenomenon and the relaxation occur due to the presence of space charges. Figure 9 (9(a), 9(b) and 9(c)) displays the graph between $\acute{Z}/\acute{Z}_{max}$ and frequency, which shows broadening of the peak with increasing temperature and milling time. It is due to the presence of electrical processes as the relaxation time expands [30, 38-42]. Figure 10 shows Nyquist plot (real part of impedance versus imaginary part of impedance) taken over a frequency. From the plot, we observe a single semicircular arc which contributes to presence of single phase and also, presence of grain interior property of material. The fitting of the Nyquist graphs was performed with fitting error less than 5% from a Z view software and the corresponding circuit and values are shown in Table 4 indicating the presence of thermally activated conduction processes inside grains and at grain borders.

Plot between ac conductivity and $1000/T$ displayed in Figure 11 at 1 kHz for different milling hours. The conductivity obeys the thermally activated properties with temperature and follows the Arrhenius relation:

$$\sigma_{ac} = \sigma_0 e^{-\frac{E_a}{kT}} \tag{7}$$

where σ_0 is the pre-exponential factor, E_a is the activation energy, k is the Boltzmann constant and T is the absolute temperature. It is observed from the graph that conductivity increases as temperature increases which shows the NTCR (Negative temperature coefficient of resistance) behavior of the material. The presence of distinct types of conduction processes with different activation energies is suggested by each plot with varied slopes in different temperature ranges and the oxygen vacancies can be one of the charge carriers in the case of ferroelectric materials. The energy needed for the polaron to jump over grain boundaries is known as activation energy. The polarons receive enough thermal energy to activate and cross the barrier as the temperature rises [30,33]. The values of the activation energy of different milling hours specified in the Table 5.

The material's electrical characteristics improve as we move into the nano range by increasing the milling process, indicating that it is suitable for tenable and energy storage devices. [43, 44]. We have done the experiments for realizing the better properties of the tungsten doped Barium titanate. However, computational studies [45-49] can also be conducted for scanning the whole samples and realizing the best performance of the devices based on required physical properties.

4. Conclusion

The tungsten doped Barium titanate was prepared by ball milling technique for three different milling hours to observe the microstructural, dielectric and impedance properties. XRD reveals the single tetragonal phase formation with perovskite structure and SEM analysis exhibits the formation of well-defined grains as increase in milling hours. The dielectric studies revealed the presence of diffuse nature of phase transition from ferro to paraelectric at $T_c = 80$°C which is related to tunability application. Also, the dielectric constant increases with milling time, thus we obtain the maximum dielectric constant value after 30 hours of milling which is suitable for energy storage applications. Nyquist plots in impedance studies exhibit a single semi-circular arc indicating the single-phase contribution to the sample's electrical characteristics and also the presence of grain inner property of material. It is also observed that with increasing temperature, the bulk resistance falls and the conductivity rises whereas the activation energy increases with increasing milling hours confirming the NTCR characteristics.

The examination of all results as we move towards high milling time, the nano range material formed which led to the conclusion that the nature of the dopants, the sintering regime, and the microstructure created by the chosen

synthesis processes were all significant for the production of appropriate ferroelectric properties and are suitable for their use in future ferroelectricity-based devices such as opto-electronics, tunable and storage devices.

Conflict of interest statement:
The authors declare that they have no conflict of interest.

References